Reconstruction of electrostatic field at the interface leads to formation of two-dimensional electron gas at multivalent (110) $LaAlO_3/SrTiO_3$ interfaces

Yin-Long Han,[1,*] Yue-Wen Fang,[2,*] Zhen-Zhong Yang,[3,*] Cheng-Jian Li,[1] Lin He,[1] Sheng-Chun Shen,[1] Zhong-Zhong Luo,[1] Guo-Liang Qu,[1] Chang-Min Xiong,[1] Rui-Fen Dou,[1] Xiao Wei,[4,†] Lin Gu,[3,5,‡] Chun-Gang Duan,[2,§] and Jia-Cai Nie[1,‖]

[1]*Department of Physics, Beijing Normal University, Beijing 100875, People's Republic of China*

[2]*Key Laboratory of Polar Materials and Devices, Ministry of Education, East China Normal University, Shanghai 200062, People's Republic of China*

[3]*Laboratory for Advanced Materials & electron Microscopy, Beijing National Laboratory for Condensed Matter Physics, Institute of Physics, Chinese Academy of Sciences, Beijing 100190, People's Republic of China*

[4]*Department of Materials Science and Engineering, Zhejiang University, Hangzhou 310027, People's Republic of China*

[5]*Collaborative Innovation Center of Quantum Matter, Beijing 100190, People's Republic of China*

(Received 20 January 2014; revised manuscript received 5 June 2015; published 15 September 2015)

The interfacial atomic arrangement, which is different from that in the bulk form of the heterojunction, can induce a reconstruction of electrostatic field at the interface. For conventional semiconductor heterointerfaces, it is known that such reconstruction results in band bending, creating a quantum well in which the two-dimensional electron gas (2DEG) is formed. In this article, we show that this mechanism still works in a multivalent oxide heterojunction: for (110) $LaAlO_3/SrTiO_3$ (LAO/STO) heterojunctions, the coexistence of La and Ti in ABO_3 perovskite unit cells at the interface reduces the valence of Ti, generating a local field leading to band bending in the interfacial STO layers. The extra free electrons are trapped in this bent conduction band forming a 2DEG. It unifies two independent mechanisms for 2DEG at LAO/STO interfaces, the "polar catastrophe" model and the "$La_{1-x}Sr_xTiO_3$" layers model, and is expected to end the decade-old controversy. This study opens insight into atomic-scale band engineering to control the behavior of complex oxide heterojunctions.

DOI: 10.1103/PhysRevB.92.115304 PACS number(s): 73.20.−r, 68.35.−p

I. INTRODUCTION

The ability to grow atomic-scale perovskite oxide heterostructures has led to tremendous exciting findings in the past decades [1,2]. In particular, the discovery of highly conductive quasi-two-dimensional electron gas (2DEG) formed at the interface between two insulating oxides, i.e., (001) $LaAlO_3/SrTiO_3$ (LAO/STO) [3], has attracted much attention [4–21]. It is one of the most important emergent phenomena at oxide interfaces, and could have potential device applications [1,10]. Novel quantum states, such as 2D superconductivity [11–13], ferromagnetism [14–18], and their coexistence [19–21], are also observed at this interface.

Despite having been extensively studied for almost ten years, the origin of the 2DEG at (001) LAO/STO interfaces is still under debate [4,22–27]. So far the mechanisms are divided into mainly three schools. (I) The most popular mechanism is the polar catastrophe model [3,4]. In order to avoid divergence of the electrostatic potential induced by polar discontinuity at the $(LaO)^+/(TiO_2)^0$ interface, at a critical thickness (t_c) of 4 monolayer (ML) of LAO [5,22,28–30], half an electron is transferred from LAO to the interface to form the 2DEG, so that Ti^{3+} appears and the accumulated electric field in LAO is eliminated. However, within t_c, the predicted electric field was not found [29,31,32], and unexpected Ti^{3+} signals appeared instead [31,33,34]. Beyond t_c, a built-in field across LAO still exists [25]. Moreover, recent experiments indicate that even at (110) LAO/STO interfaces, where both LAO and STO stacking have the sequence $(ABO)^{4+}/(O2)^{4-}$ avoiding any polar discontinuity in the ionic limit [35,36], unexpectedly high mobility metallic conductivity was found [36,37]. Soon, the 2D superconductivity at (110) LAO/STO interfaces was also reported [38,39]. These observations place the most popular mechanism in doubt. (II) "$La_{1-x}Sr_xTiO_3$" intermixing layers, observed at the (001) LAO/STO interfaces in many studies [24,40–43], were also used to explain the conductivity based only on the fact that the $La_{1-x}Sr_xTiO_3$ bulk is metallic between $x = 0.05$ and 0.95 [44,45], but the microscopic physical nature of this $La_{1-x}Sr_xTiO_3$ intermixing layer is still unclear and little attention has been paid to this mechanism until now. (III) Oxygen vacancies in STO indeed can contribute extra carriers [23,27,46,47] but may be not the underlying origin, because the conductivity still remains for the postannealed samples [27], and the *p*-type [(001) LAO/SrO-STO] interfaces would be conductive if oxygen vacancies were the mechanism [3]. To sum up, the biggest controversies mainly focus on the former two mechanisms, which have been considered to be independent or even mutually exclusive ones and debated for almost ten years. So what exactly is the key to forming 2DEG at LAO/STO interfaces?

As mentioned above, if the most widely accepted "polar catastrophe" mechanism works, the (110) LAO/STO interfaces should not be conductive but the fact is just the opposite. So it is very important to deeply investigate the (110) LAO/STO interfaces and to figure out the mechanism of the quasi-2DEG of this interface which is expected to provide fruitful physics to understand the origin of the 2DEG at (001) LAO/STO interfaces. Nevertheless there has been little attention paid to this theme until now. For conventional semiconductor

*These authors contributed equally to this paper.
†mseweixiao@zju.edu.cn
‡l.gu@iphy.ac.cn
§wxbdcg@gmail.com
‖jcnie@bnu.edu.cn

heterojunctions, the 2DEG is generated at a potential well created by band bending due to the presence of an electrostatic field at the interfaces. In this article, we performed combined studies of x-ray photoelectron spectroscopy (XPS), high-angle annular dark-field scanning transmission electron microscopy (HAADF-STEM), atomic-resolution electron energy loss spectroscopy (EELS), and density functional theory (DFT) calculations to investigate the band alignment and interfacial atomic structure of (110) LAO/STO interfaces. Based on these results, we show that the scenario accounting for a 2DEG at conventional semiconductor heterointerfaces still works here. The coexistence of La and Ti at the interface and the resultant band bending in STO should be key to forming 2DEG at LAO/STO interfaces.

II. EXPERIMENTS AND RESULTS

A. Sample preparation and basic characterization

The as-received (110) STO substrates were treated at 1050 °C for 2 h under oxygen atmosphere [48], atomically flat (110) STO surfaces were obtained [Fig. 1(a)]. The substrate was heated from room temperature to 750 °C in 0.1 mbar of O_2, then the LAO layer was grown in 10^{-4} mbar mbar of O_2 by pulse laser deposition (PLD). The laser pulses were supplied by a KrF excimer sources ($\lambda = 248$ nm) with an energy density of 1.5 J/cm^2 and a frequency of 1 Hz. After deposition, every sample was cooled down in oxygen rich atmosphere to reduce the formation of oxygen vacancies [33,36,49]: $P_{O2} = 0.3$ mbar mbar from 750 °C to 600 °C and $P_{O2} = 200$ mbar from 600 °C to room temperature, with a dwell time of 1 h at 400 °C.

After deposited LAO film the atomically flat terraces were preserved perfectly as shown in Fig. 1(b). The typical XRD patterns of the (110) LAO/STO heterojunctions are show in Fig. 1(d). The two higher sharp peaks are the (110) and (220) orientation peaks of the single crystal STO substrate. LAO and STO are perovskite structure and have very similar lattice constant, so their (*ll*0) XRD peaks are very close. It is very hard to get independent and clear (*ll*0) peaks of LAO on (110) STO substrate. But we can see clearly there are two sharp shoulders beside the main peaks of the (110) STO substrate, which correspond to the epitaxial LAO (110) and (220) XRD peaks. The detailed data of LAO (110) is shown in Fig. 1(e); clear Laue oscillations indicate that our LAO film has high lattice perfection and smooth interface. There are no other peaks except (*ll*0) ones on the XRD data, confirming that we get single phase (*ll*0) LAO epitaxial film on (110) STO substrate.

The x-ray reflectivity (XRR) data of a sample with 5000 laser pulses is shown in Fig. 1(c). We used *REFSIM* software to simulate the XRR data. The simulation (red curve) corresponds to a LAO thickness of 22.632 nm. We can also get the thickness from the Laue oscillations [Fig. 1(e)]; the result is about 21.036 nm. The average value of the two results is 21.834 nm. So the growth rate is estimated to be about 1 monolayer per 60 laser pulses. The LAO layer thickness was determined by the number of laser shots and the calibrated growth rate.

The measurement of the sheet resistance of the samples was performed by using eight-contact arrangement in Hall geometry on the samples shown in the inset of Fig. 2(a).

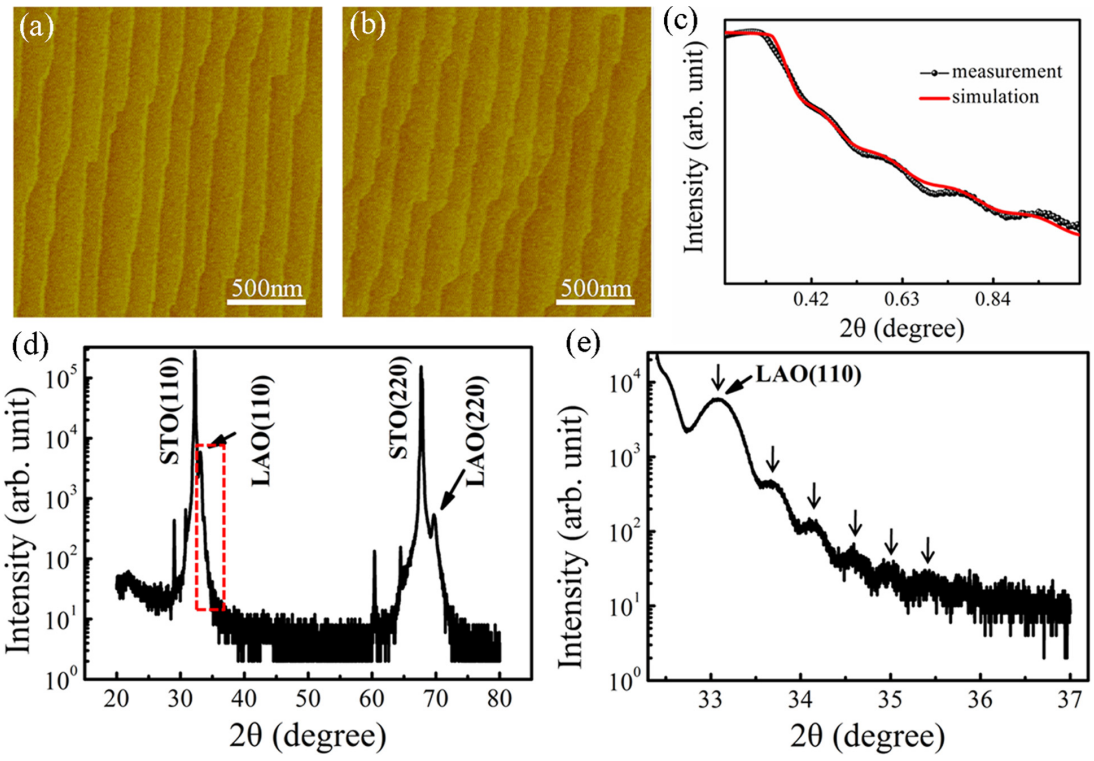

FIG. 1. (Color online) (a) and (b) Representative topographic AFM images of a treated STO substrate and a 8 ML LAO thin film on the same substrate. (c) X-ray reflectivity data of a LAO thin film, with a thickness of 22.632 nm determined by simulation of the measured data. (d) XRD patterns of the same sample in (c). (e) Enlarged view of the red-box-enclosed part of (c); clear Laue oscillations are indicated by the arrows.

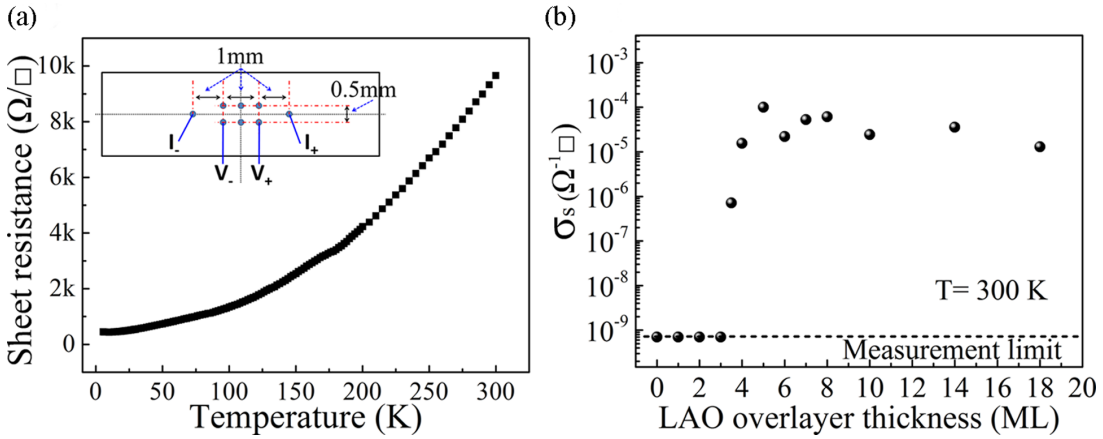

FIG. 2. (Color online) (a) Temperature dependence of the sheet resistance. The inset shows the eight contacts arranged in Hall geometry on the sample. (b) Sheet conductance plotted as a function of the LAO overlayer thickness.

The contacts were formed by using 25-micrometer-diameter Al wires wedge bonding directly connected to the sample interfaces. A typical temperature dependence of the sheet resistance of a sample with 5 ML LAO overlayers is shown in Fig. 2(a). Clear metalliclike behavior is observed. An insulator to metal transition clearly shown in Fig. 2(b) indicates that all samples have metallic conduction when the LAO thickness is more than three ML. The sheet resistance, the estimated carrier density, and mobility at both room temperature and low temperature of our samples (data not shown) are basically consistent with the former reports of the (110) LAO/STO interfaces [36–39].

B. Band bending and band alignment

The samples were immediately transferred to the XPS chamber after deposition, and no surface treatment was performed prior to measurement. The XPS data were obtained using an ESCA Lab250 electron spectrometer (Thermo Scientific Corporation) with monochromatic 150 W Al $K\alpha$ ($h\nu =$ 1486.6 eV) radiation as the x-ray source; the ultimate energy resolution is 0.45 eV. The base pressure was about 10^{-10} mbar, and the measurements were done at room temperature. The XPS spectra were collected at normal emission to the surface of the samples. A negative 4 V bias was applied to the sample to overcome the work function of the analyzer. The charge effect was stable for a certain sample by using a two guns system, a low-energy electron gun and a low-energy ion flood gun, to compensate the extra charge during the measurements. The XPS data were processed using *Thermo Avantage* software. All core level peaks were fitted using a smart background and Gauss-Lorentz mix line shapes. We reference all binding energy relative to the Fermi level (E_F) and all the binding energy below the E_F is positive. The binding energy of each sample was referenced to the C 1*s* line at 284.8 eV.

Band bending of the heterojunction can be determined quantitatively by the core level shift with changing the overlayer thickness [49]. Here we use Ti $2p_{3/2}$ and Al $2p$ core level shift to determine the band bending in STO and LAO of (110) LAO/STO heterojunctions, respectively, by changing the LAO overlayer from 0 ML to 18 ML. The 0 ML sample was a bare (110) STO substrate which was transported into PLD chamber, exposed to the condition of the growth process, being maintained for 10 min without LAO deposition. Figure 3(a) presents Ti $2p_{3/2}$ and Al $2p$ core level spectra as a function of LAO film thickness which indicates that Ti $2p_{3/2}$ shifts to higher binding energy while Al $2p$ shifts to the lower as the LAO thickens from 0 ML to 18 ML. The quantitative results of core level shift are shown in Fig. 3(b). The Ti $2p_{3/2}$ peak shifts upward from 0 ML to ∼4 ML, then saturates at about 7−10 ML, and, surprisingly, moves upward again over ∼10 ML. Explanation of this upward-tail phenomenon can be found in Appendix A. The final shift of Ti $2p_{3/2}$ is about 0.5 ± 0.03 eV. Therefore, there is downward band bending of about 0.5 ± 0.03 eV at STO side toward the interface. The Al $2p$ core level shifts downward about 0.77 ± 0.03 eV, from 0.95 ± 0.02 eV to 0.18 ± 0.02 eV [Fig. 3(b)], with an increase of the LAO overlayer thickness, and the final shift is about 0.95 ± 0.07 eV in reference to that of bulk LAO. So the LAO band also bends downward toward the interface.

The valence band offset (VBO) of heterojunction can be determined by using a pair of core levels from substrate and thin film, respectively [31]. We use the Ti $2p_{3/2}$ in STO substrate and the Al $2p$ in LAO overlayer to determine the VBO of samples with different LAO overlayer thickness (for details, see Appendix B). The VBO value [Fig. 3(c)] is about -0.68 ± 0.15 eV for 1 ML sample, increases to positive more than 4 ML, then slowly rises to about 0.6 ± 0.15 eV at 18 ML. Combining with the above band bending analysis, a band alignment of the (110) LAO/STO heterojunctions is shown in Fig. 3(d). The band alignment well explains the critical thickness for appearance of the metallic states at (110) LAO/STO interfaces: the STO band bends more as LAO thickens, metallic conduction appears when Fermi level E_F is located inside the conduction band of the STO with LAO thickness over 3 ML.

The downward bent conduction band of STO [circled by red dashed line in Fig. 3(d)] due to downward band bending at (110) LAO/STO interfaces is very similar to that of (001) LaO/TiO_2-STO interfaces but is absent for (001) LAO/SrO-STO interfaces according to the study of Yoshimatsu [49]. The downward bent conduction band is a potential well for electrons. Its existence for both (110) LAO/STO and (001) LaO/TiO_2-STO interfaces indicates that

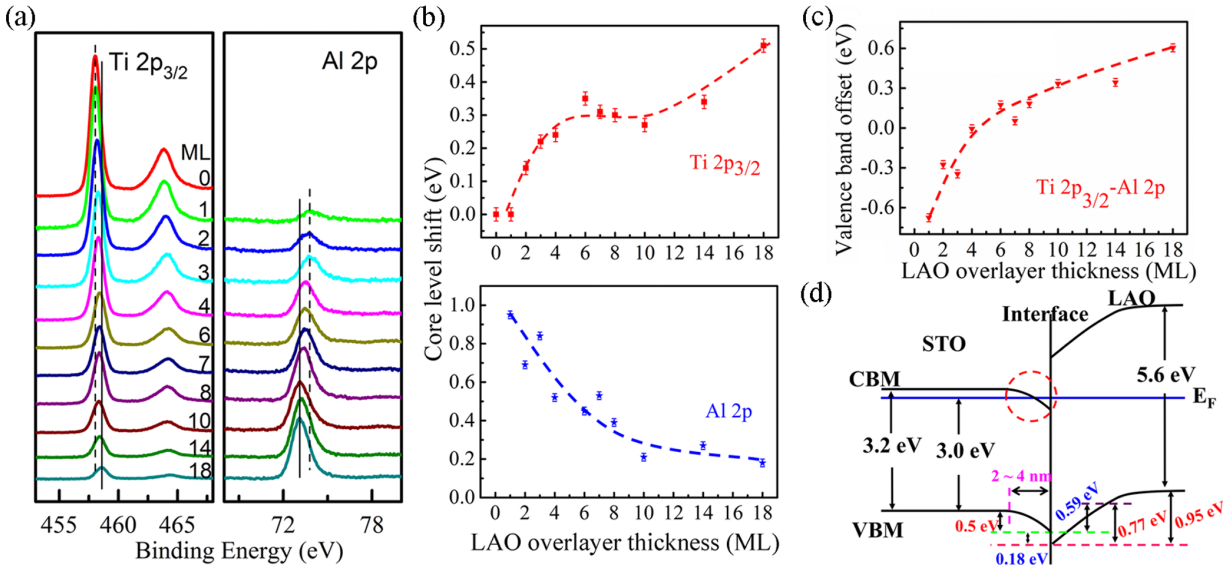

FIG. 3. (Color online) Band alignment of (110) LAO/STO based on band bending and valence band offset. (a) Ti $2p$ and Al $2p$ core level spectra of (110) LAO/STO vs LAO thickness. (b) Core level shift of Ti $2p_{3/2}$ and Al $2p$ as a function of the LAO overlayer thickness. Ti $2p_{3/2}$ energy values were subtracted by that of 0 ML sample, single crystal substrate. Al $2p$ energy values were subtracted by that of bulk (30 nm) LAO sample. (c) Valence band offset with different LAO overlayer thickness. Dashed lines in (b) and (c) are guides to the eye. (d) The detailed band alignment of (110) LAO/STO interfaces deduced from results of (b) and (c).

extra free electrons would be trapped inside the quantum well to form a 2DEG. That the observed band is almost flat or bent a little bit upward in (001) LAO/SrO-STO interfaces [49], explains the absence of a 2DEG.

There may be some carriers induced by x ray during the measurements which should not only flatten the potential buildup in the LAO overlayer, but should also reduce the band bending or confining potential for the carriers in the STO substrate. Slooten *et al.* [50] had tried to deal with this photon doping problem of the x ray. While they concluded that a black or white proof on the issue of the possible effect of photodoping is not possible at this stage. As they said in their study, the band bending and the band alignment determined by the ML-by-ML XPS measurements are to be taken seriously here.

C. Interfacial atomic structure

Next, HAADF-STEM and atomic-resolution EELS investigations to examine the interfacial atomic structure of (110) LAO/STO heterojunctions were made. The STEM cross-sectional sample was prepared by conventional TEM sample preparing method. First, thinning and polishing the both sides of bonded sample by SiC and diamond waterproof papers. Then the thinned and polished sample was dimpled to submicron to several micrometers. At last, ion milling was carried out to make the sample satisfy the requirement for STEM observing. During the ion milling process, the cold stage and relatively low energy ion beam were used to prevent atomic diffusion process. Within the STEM technique, the contrast of the HAADF image exhibits an approximately $Z^{1.7}$ dependency, where Z represents the atomic number. Therefore, the interface of LAO/STO (marked by green arrows) can be clearly seen in HAADF image [Fig. 4(a)] because of the big difference of Z numbers between La, Sr, and Ti. It can be seen the boundary of LAO/STO is in order and dislocation free, which means that the epitaxial LAO/STO film has a relative high quality. While, in Fig. 4(a), the coexistence of La and Ti in ABO_3 unite cells at the interface can be observed by the image contrast, where the brighter, the bright, and the blue spots represent La, Sr, and Ti atoms, respectively; moreover, we can clearly observe obvious transition layers (marked by asterisks) from the line profile [Fig. 4(c)]. This coexistence is also further confirmed by atomic resolution EELS line scanning results [Figs. 4(d) and 4(e)]. More precisely, it can be seen that the coexistence extends into STO for at least 2 ML [Fig. 4(g)].

Intensity vs lateral position [Fig. 4(h)] also supports the above conclusions. The layer 1 and layer 5 are LAO and STO, respectively. The intensity of layer 2 being almost the same to that of layer 1 indicates that this layer is LAO, while that of layer 3 decreasing obviously but being much stronger than that of layer 5 indicates that the La atoms occupy the Sr sites in the first layer of STO substrate forming the coexistence of La and Ti in ABO_3 unit cells at the interface. The intensity of layer 4 being still stronger than that of layer 5 also proves that the coexistence extended into STO substrate for at least 2 ML. The intensity curves also indicate that the coexistence of La and Ti at the right part of the image is more and extends deeper into STO than that of the left part. This shows the coexistence is not uniform at the interface which is the reality of the situation and does not impact the conclusions.

Actually, to our surprise, the intrinsic coexistence (i.e., sharp interface) of La and Ti in a form of a $LaTiO_3$ (LTO)ML exists naturally at the conductive (001) LaO/TiO_2-STO interfaces [labeled by a red dashed ellipse in Fig. 6(g)], but is absent at (001) LAO/SrO-STO insulator interfaces. So, does the coexistence of La and Ti at the interface induce the downward band bending and further induced the 2DEG at LAO/STO interfaces?

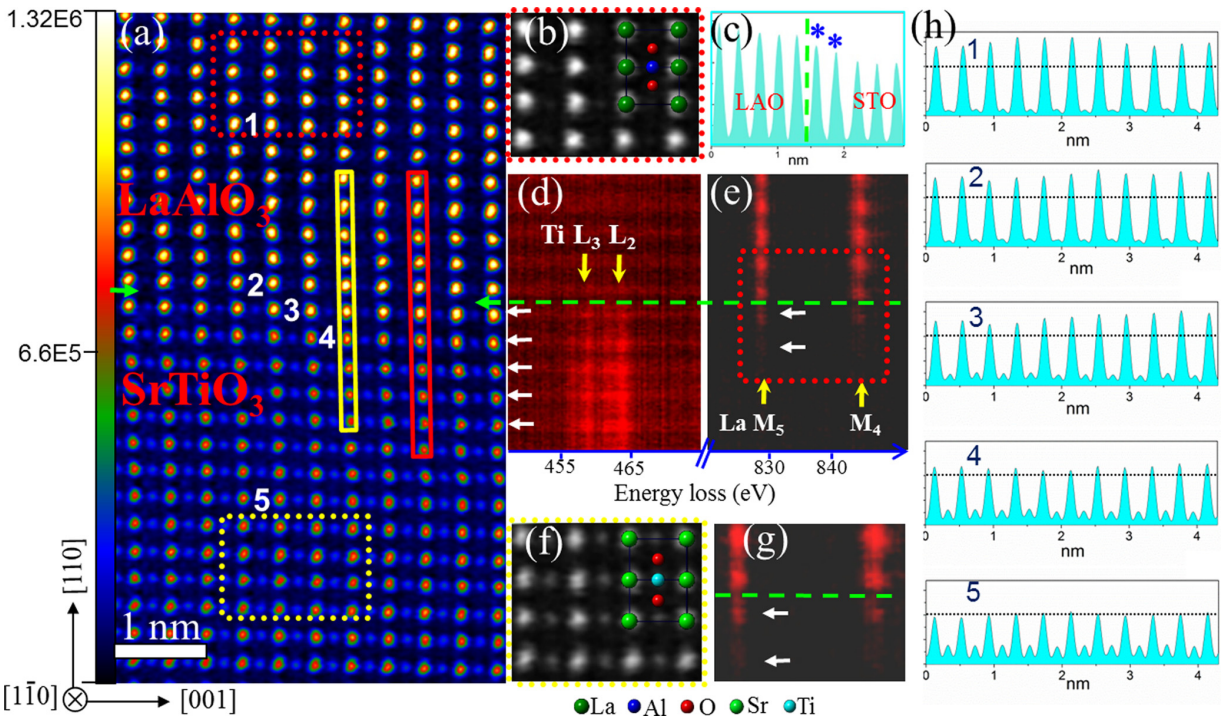

FIG. 4. (Color online) Atomic structure of (110) LAO/STO heterojuntions. (a) HAADF-STEM image of (110) LAO/STO heterojunction with an intensity scale bar left. Spherical aberration-corrected JEM-ARM200F (S)TEM is used in this observation. (b) and (f) Enlarged view of uncolored LAO and STO corresponding to the red and yellow dashed box areas, respectively, in (a). (c) Line profile corresponding to the yellow box area in (a). Atomic resolution EELS line scanning spectra of Ti $L_{2,3}$ (d) and La $M_{4,5}$ (e) taken from the red box area perpendicular to the interface in (a). (g) Enlarged view of the red dashed box area in (e). The interface is indicated by the green arrows in (a) and dotted line in (c), (d), (e), and (g). White arrows mark atomic layers. (h) The intensity vs lateral position of the layers marked by numbers in (a). The data scale bars of the intensity (y axis) of the five layers are the same. The black dashed lines indicate the values of the intensity of Sr atoms of layer 5 in STO.

D. Density functional calculations

To answer this, we performed DFT calculations of electronic structure on both a sharp (110) LAO/STO supercell [Fig. 5(a)] and a (110) $LaAlO_3/LaTiO_3$-$SrTiO_3$ (LAO/LTO-STO) supercell [Fig. 5(b)] in which Sr atoms in the top layer of STO are completely substituted by La atoms. In the DFT calculation, the exchange-correlation potential is treated in local density approximation (LDA) and the projected augmented wave method is used with a plane wave basis set as implemented in the Vienna Ab initio Simulation Package (VASP) [51]. A kinetic energy cutoff is set to be 500 eV for the plane wave basis and the Brillouin zone integration is carried out using Monkhorst-Pack grid of $12\times8\times2$ k points in combination with the tetrahedron method. The LDA optimized bulk lattice constants are 3.874 and 3.742 Å for the STO and the LAO bulk, respectively, which are slightly underestimated with respect to their experimental values (3.905 and 3.789 Å). For the optimization, we fix the in-plane lattice constant of supercell at the relaxed lattice constant of STO bulk, namely 3.874 Å, and then perform relaxation of all the coordinates of atomic positions along the c direction perpendicular to the interface until the Hellmann-Feynman forces on each atom are less than 2 meV/Å. The mechanical interface stability of both supercells is estimated by calculating their work of separation [52,53]. The results, 8.98 J/m^2 for sharp (110) LAO/STO and 9.36 J/m^2 for (110) LAO/LTO-STO, clearly show the structure is energetically in favor of a (110) LAO/LTO-STO supercell, which supports the observed coexistence of La and Ti in our STEM and EELS observations (Fig. 4).

The layer projected density of states is presented in Fig. 5. A perfect (110) LAO/STO supercell is an insulator and the band is flat [Fig. 5(a)]. For a (110) LAO/LTO-STO supercell, however, the band bends downward toward the interface at both sides of the interface with the E_F located inside the conduction band of STO which indicates that metallic conductivity appears [Fig. 5(b)]. In addition, results for a (110) $LaAlO_3/La_{0.5}Sr_{0.5}TiO_3$-$SrTiO_3$ supercell whose interfacial Sr atoms are partially replaced by La also suggest band bending of STO (data not shown) though it is not as remarkable as that in Fig. 5(b), hinting that the concentration of La ion acts as an extraordinary role in forming of the band bending. Surface x-ray diffraction results by Willmott *et al.* [24] indicate that $La_{1-x}Sr_xTiO_3$ intermixing layers exist at the (001) LaO/TiO_2-STO interface. According to their DFT calculation, there is a flat or a slightly upward bent band in STO for (001) LAO/SrO-STO interfaces, while a downward band bending at the STO side for both sharp and intermixed (001) LaO/TiO_2-STO interfaces is shown in Fig. 4 of Ref. [24].

According to the DFT calculation results, we can conclude that the coexistence of La and Ti at the interface indeed induce a downward bent conduction band of STO, form a potential well, and then free electrons are trapped to form 2DEG.

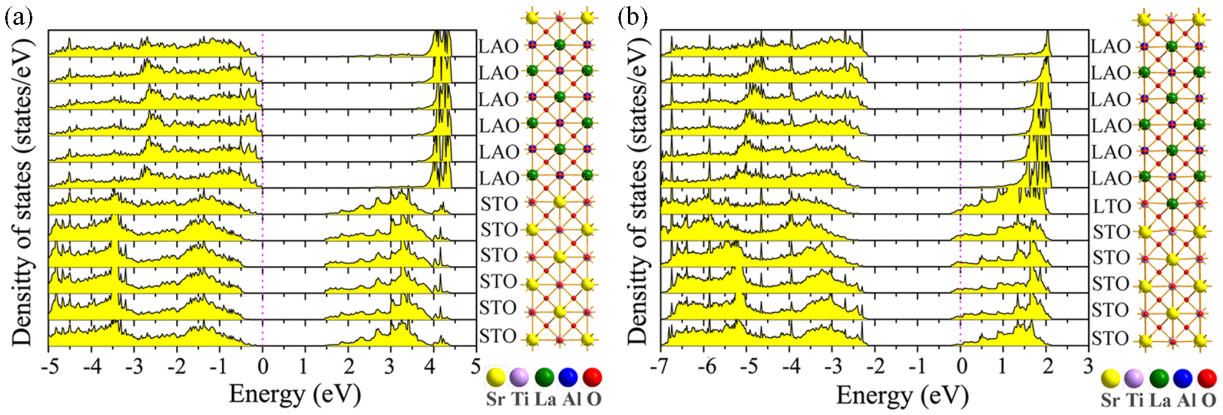

FIG. 5. (Color online) Comparison of layer projected density of states. (a) and (b) Layer projected density of states for perfect (110) LAO/STO and (110) LAO/LTO-STO supercells, respectively. Zero is the reference for the Fermi level. The atomic models are shown in the right.

E. Reconstruction of the electrostatic field

Why does the coexistence of La and Ti at the interface induce the downward bent band in STO? This is explained by an electrostatic model. Ti is a multivalent element whose valence is +4 in STO but +3 in LTO. So the La substitution for Sr in a STO unit cell could release electrons to Ti to reduce its valence, which is supported by Ohtomo *et al.* [54], Okamoto *et al.* [55], and Jang *et al.* [56]. The change of the valence of Ti can induce a reconstruction of the electrostatic field at the interface. We assume that the valence of Ti would decrease from +4 to +3 in proportion to the ratio of La/Sr surrounding the Ti-O octahedron as shown in Fig. 6(a). According to this simple assumption, for the specific (110) LAO/LTO-STO interface, as shown in Fig. 6(d), the valence of Ti decreases

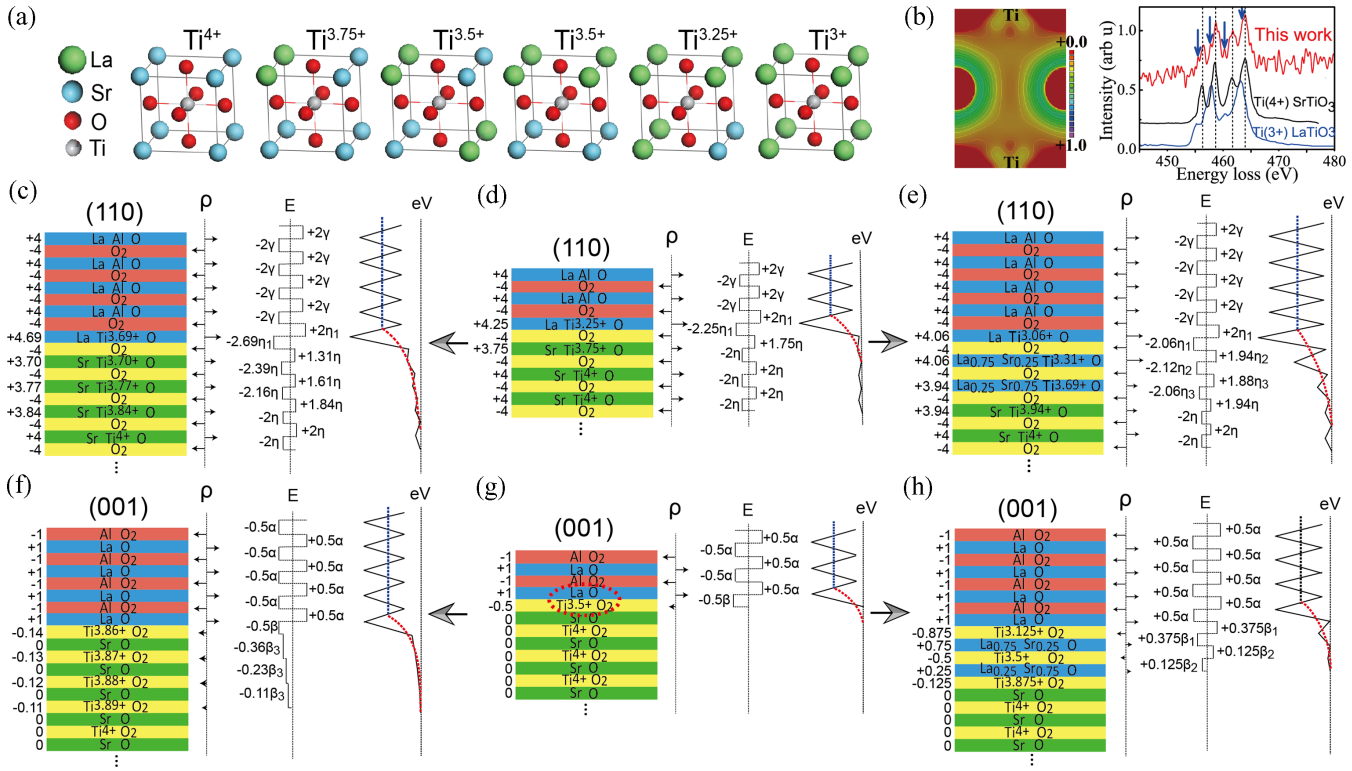

FIG. 6. (Color online) Electrostatic models of band bending in STO of both (001) and (110) LAO/STO interfaces. (a) The valence of Ti will decrease from +4 to +3 in proportion to the ratio of La/Sr surrounding the Ti-O octahedron. (b) Left: charge density difference of interfacial titanium atoms. Right: detailed view of the Ti $L_{2,3}$ edges for the Ti site at the interface layer of our (110) LAO/STO sample. (d) and (g) are for (110) LAO/LTO-STO and sharp (001) LAO/STO, respectively, where the intrinsic coexistence of La and Ti exists. (c) and (f) are the situation considering the diffusion of the electrons based on (d) and (g). (e) and (h) are the results after inserting two layers of $La_{1-x}Sr_xTiO_3$ in (d) and (g), corresponding to the extrinsic coexistence of La and Ti. We calculated the values of static field and potential energy by assuming an infinite plane-parallel capacitor structure of atomic layers. α, β, γ, and η are constants deduced by calculation (see Appendix E for details). The valences of La, Al, O, and Sr are not marked out.

because of the coexistence of La and Ti in an ABO_3 unit cell, and then the net charge (ρ) changes. Thus it induces a local asymmetric electric field (E) which leads to a decrease of the potential energy (eV) toward the interface, giving downward band bending of STO as the red dashed lines show. Sharp (001) LAO/STO interfaces, where the intrinsic coexistence of La and Ti exists, has similar results [Fig. 6(g)]. We define the coexistence of La and Ti at the specific (110) interface [Fig. 5(b)] as intrinsic coexistence [57]. Thus intrinsic coexistence of La and Ti at the interface induces the downward band bending for both (001) and (110) LAO/STO heterojunctions. But the region of the bending is narrow. Actually, electrons supplied by the La occupation of the Sr sites would diffuse away from the interface into inner STO layers; consequently, the valence of Ti lying further away from La would also decrease. This is supported by Ohtomo *et al.* [54] and Jang *et al.* [56]. Assuming the electrons diffuse into STO with an attenuation function similar to that of Ref. [54], the region of band bending obviously enlarges [Figs. 6(c) and 6(f)]. On the other hand, the extrinsic coexistence of La and Ti due to La diffusion which may occur during fabrication of the heterojunctions [24,41], e.g., inserting two layers of $La_{1-x}Sr_xTiO_3$ under the interface, also enlarges the region, as shown in Figs. 6(e) and 6(h) (no electronic diffusion). If both of these two factors act together, the region of band bending would be enlarged more. That is why the observed width of band bending of the (110) LAO/STO samples, 2−4 nm [shown in Fig. 3(d), and see Appendix C for method; this confinement scale is comparable to that of (001) LAO/STO interfaces according to the systematic calculation [58] and many experiments [4,33,59]], is larger than that schematically shown in Fig. 6(c) [intrinsic coexistence (electronic diffusion)] and Fig. 6(e) [intrinsic and extrinsic coexistence (atomic diffusion)], ∼1.1 nm [∼4 ML of (110) STO]. Thus this electrostatic model well explains, for both (001) and (110) LAO/STO heterojunctions, why the coexistence of La and Ti at the interface, whether intrinsic coexistence alone or together with extrinsic coexistence, indeed can induce downward band bending in STO.

The detailed EELS of Ti $L_{2,3}$ shows that there is Ti^{3+} [marked by blue arrows in Fig. 6(b), right] at our (110) LAO/STO interfaces. The charge density difference [Fig. 6(b), left], acquired by subtracting the charge density of the interfacial STO layer [Fig. 5(a)] from that of the interfacial LTO layer [Fig. 5(b)], indicates an increase of Ti charge density and a consequent decrease of the valence of Ti. Furthermore, by analyzing the Bader charges [60,61] of interfacial atoms in perfect (110) LAO/STO and (110) LAO/LTO-STO supercells contrastively, we find that the Bader charges of Ti increase from 1.3573 to 1.3802, while those of La decrease from 8.9506 to 8.9404. This charge transfer behavior unambiguously indicates that there exists mixed valence of +3 and +4 in Ti due to the coexistence of La and Ti. Several experimental studies (see, e.g., Refs. [4] and [33]) also have shown that Ti^{3+} exists at (001) LaO/TiO_2-STO interfaces. All these results indicate that a reconstruction of the electrostatic field indeed occurs at both (001) and (110) LAO/STO interfaces. The calculated values of band bending according to Fig. 6 are about 0.337 eV and 0.52 eV for (001) and (110), respectively, which agree well with those of the experimental values [0.25 eV for (001) in Ref. [49] and 0.5 eV for (110) as shown in Fig. 3(d)]. These results all confirm that our model is reasonable and suitable. The band bending of LAO [for (110) LAO/STO interfaces, see our XPS and DFT results as shown in Figs. 3(d) and 5(b); for (001) LAO/STO interfaces, Guneeta *et al.* reported that there is electric field across LAO which must generates band bending of LAO [25]] could also be well explained by the above electrostatic model (see Appendix D).

III. DISCUSSION

Based on our results of the band alignment, the interfacial atomic structure, the DFT calculations and the electrostatic models at (110) LAO/STO interfaces, we propose the understanding of the basis to 2DEG at (110) LAO/STO interface: the intrinsic coexistence alone or together with the extrinsic coexistence of La and Ti in ABO_3 perovskite unit cells at the interface, reduces the valence of Ti, and then generates a local electric field on the STO side, and further results in downward band bending of STO. The extra free carriers, basically from the coexistence of La and Ti or from oxygen vacancies or other defects, would be trapped in the bent STO band forming a 2DEG. So the coexistence of La and Ti at the interface and the resultant downward bent conduction band of STO should be the key to the formation of 2DEG at LAO/STO interfaces. According to former results of the (001) LAO/STO interfaces mentioned in Secs. II B to II E, this understanding of the basis to 2DEG should be also suitable for (001) LAO/STO interfaces.

Polar catastrophe model, the most popular mechanism, claims that when the LAO thickness is greater than t_c, driven by a large accumulated electric field in LAO, the electrons transfer from LAO to STO to cause electronic reconstruction. However, this has been challenged by many studies [25,29,31–34]. In our understanding, the electron transfer takes place once La is close to Ti, not driven by the accumulated electric field. Therefore, within t_c, Ti^{3+} will appear and the accumulated large electric field in LAO cannot exist. So the challenges faced by polar catastrophe model are solved. Within the $La_{1-x}Sr_xTiO_3$ intermixing model, it had not been clearly noticed before that the $La_{1-x}Sr_xTiO_3$ intermixing layer has any relationship with electron transfer and the band bending of STO. Here we clearly demonstrate that the $La_{1-x}Sr_xTiO_3$ intermixing also stimulates electrons transfer resulting in electronic reconstruction and causes the band bending in STO for both (110) and (001) LAO/STO heterojunctions. This should be the microscopic role of the $La_{1-x}Sr_xTiO_3$ intermixing layers.

Moreover, from the point of interfacial atomic structure, the polar catastrophe model and the $La_{1-x}Sr_xTiO_3$ intermixing model correspond to the situations of the intrinsic and extrinsic coexistence of La and Ti, respectively, and the physical nature of both models is the electronic reconstruction resulted by charge transfer from La atoms to Ti atoms due to the coexistence of La and Ti at interface. So the two seemingly independent or even mutually exclusive mechanisms are unified in our understanding. In addition, the extra free electrons supplied by the oxygen vacancies may also be trapped in the quantum well resulted by the coexistence of La and Ti to participate in transport. From this point, the oxygen vacancies model could also be merged into the framework of our understanding.

Reference [37] first proposed a mechanism analogous to the "polar catastrophe" model based on ideal buckled LaO/TiO_2 layers at the (110) LAO/STO interfaces. It only corresponds to the situation of intrinsic coexistence in our understanding and does not consider the reality that the coexistence of La and Ti extends into STO for at least 2 ML, which both they and we observed. While we give comprehensive understanding of (110) LAO/STO interfaces and can also well explain the results of (001) LAO/STO interfaces that the atomic intermixing also may play a role for the conductivity: Willmott *et al.* reported that there are several $La_{1-x}Sr_xTiO_3$ intermixing layers at (001) LAO/STO interfaces and the band bending by their DFT calculations is enhanced for the intermixing model [24]; Yamamoto *et al.* compared *n*-type and *p*-type (001) LAO/STO interfaces and found that *n*-type interface has deeper intermixing, a large polarized region, and distinct degrees of band bending [43].

IV. CONCLUSIONS

In conclusion, the coexistence of La and Ti at the interface and the resultant downward bent conduction band of STO should be the key to the formation of 2DEG at LAO/STO interfaces. Furthermore, in essence, the electronic reconstruction due to the coexistence of La and Ti at the LAO/STO interface is because of the difference between the valence of La and that of Sr. So if La were replaced by other elements whose valence is different from that of Sr, electronic reconstruction and the resultant physics would be also expected in other STO based heterojunctions [56]. It highlights that precisely controlling the interfacial atomic arrangement can tune the band alignment and stimulate physics in multivalent oxide heterojunctions. Although complex oxides always are strongly correlated systems, as semiconductor concepts achieve maturity, much of the same phenomenology can be borrowed to offer more degrees of freedom for exploration [25]. This work paves broad avenues of atomic-scale engineering to tailor fascinating behaviors of complex oxide heterojunctions and to design oxide electronic devices.

ACKNOWLEDGMENTS

This work was supported by the Ministry of Science and Technology of China (Grants No. 2012CB921702, No. 2013CB921701, No. 2013CB922301, No. 2014CB920903, No. 2014CB921104, and No. 2014CB921002), the National Natural Science Foundation of China (Grants No. 11474022, No. 51172029, No. 91121012, No. 10974019, No. 11004010, and No. 61125403), and the Strategic Priority Research Program of the Chinese Academy of Sciences (Grant No. XDB07030200). Computations were performed at the ECNU computing center. Y.-W.F. is indebted to Zhizhou Yu for inspiring discussions.

APPENDIX A: EXPLANATION OF UPWARD-TAIL PHENOMENON

Here, we give a pretty convincing explanation [as illustrated in Fig. 7(a)] of this upward-tail phenomenon: assuming the STO band bends downward with increasing LAO thickness, and saturates for LAO more than 6 ML. The detected core level

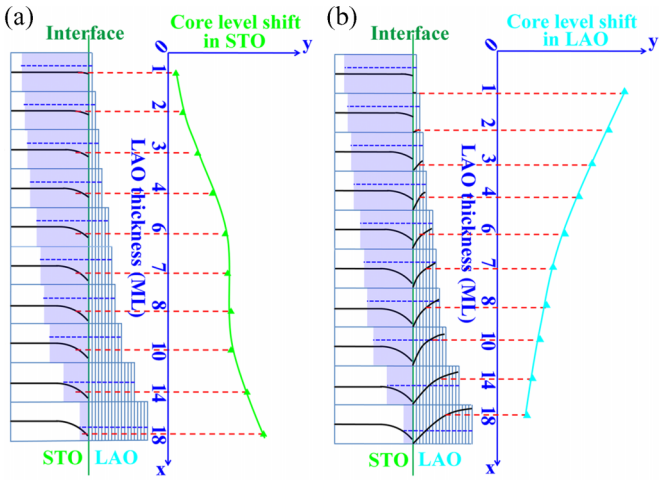

FIG. 7. (Color online) Band bending determined by core level shift. (a) and (b) The corresponding relationship between the band bending and the shift of the detected core level binding energy (DCLBE) in STO and LAO. The blue dashed lines and the shaded areas show the XPS investigation depth in heterojunction and in STO, respectively. It is obvious that the XPS investigation depth in STO shallows as LAO thickens. The black lines represent the valence band, whose bending has the same direction and value with that of core levels. The red dashed lines mark the positions of the DCLBE in the heterojunction determined by XPS measurements, which actually are average values of all core levels in the whole detecting depth. The core level shift (y axis) of DCLBE is subtracted by that in bulk STO or LAO.

binding energy (DCLBE) by XPS, however, is an average value of all core levels in the whole detecting depth. So it will shift upward within 6 ML. Between 6 to 10 ML, the band bending of STO does not change, and XPS can penetrate and detect the whole bending region of STO, so the DCLBE nearly saturates. Nonetheless, more than 10 ML, the XPS investigation depth in STO becomes thinner; the DCLBE of the STO near the interface will shift upward again although the band bending is unchanged. Based on this clarification, if the measurement was stopped at the saturation [49], the obtained shift should be smaller than the actual value. So we should perform the measurement by increasing the LAO overlayer thickness until the

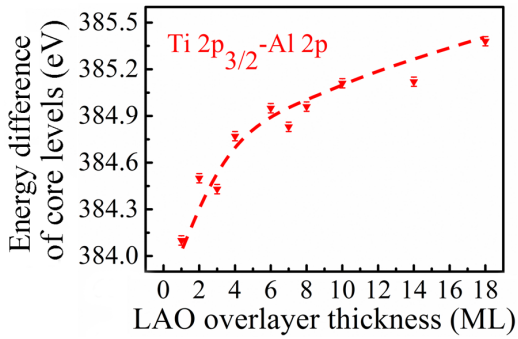

FIG. 8. (Color online) Core level energy differences. Core level energy differences of $(E_{\mathrm{Ti}\,2p3/2} - E_{\mathrm{Al}\,2p})_{\mathrm{HJ}}$ for (110) LAO/STO heterojunctions with different LAO thicknesses. The dashed lines are guides to the eye. It indicates that the LAO core level shifts about 1.2 ± 0.03 eV toward higher energy relative to those of STO.

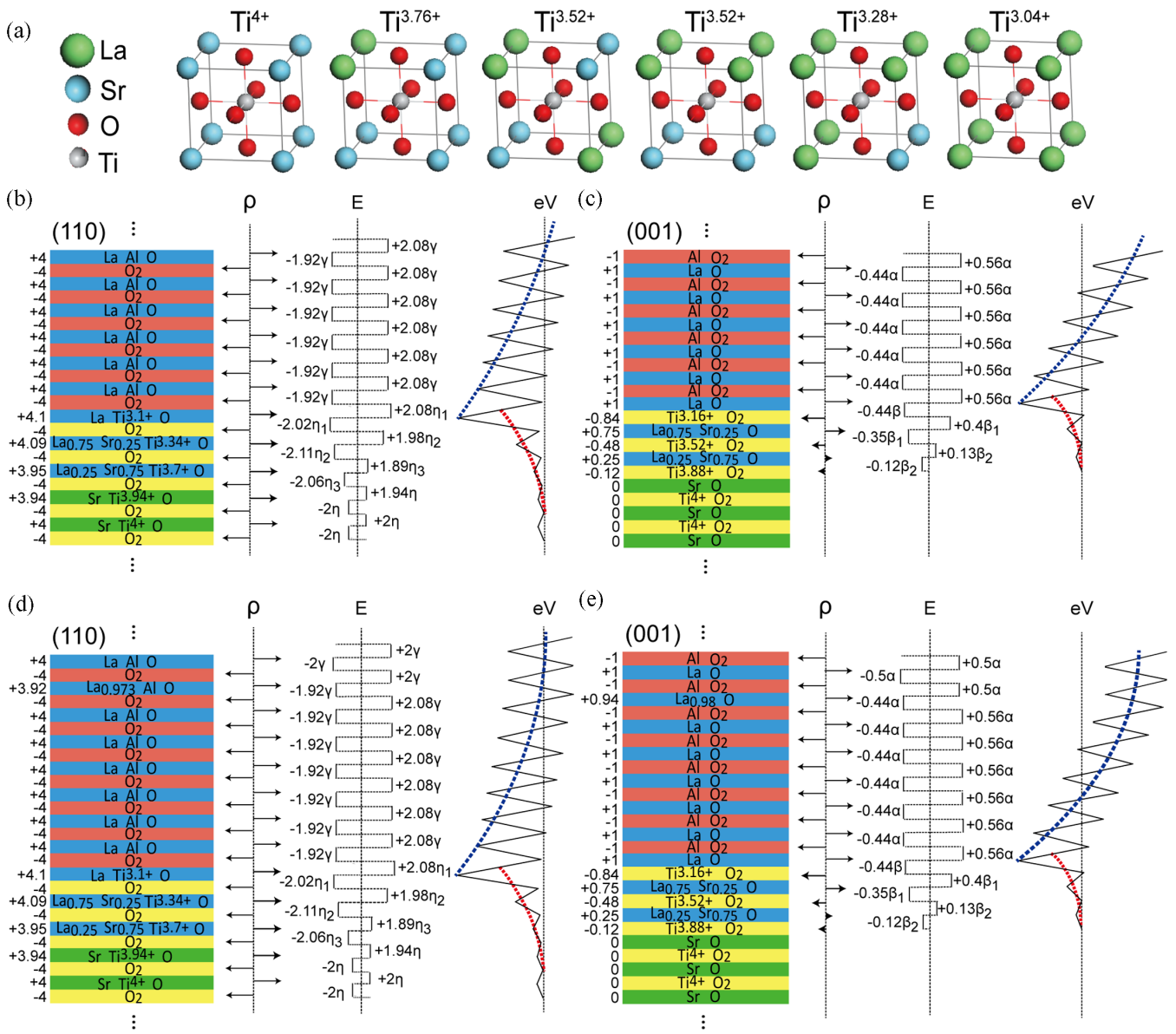

FIG. 9. (Color online) Explanation of band bending of LAO for the extrinsic coexistence of La and Ti. (a) After amending the model in the main text a little, the valence of Ti would decrease from +4 to +3.04 in proportion to the ratio of La/Sr surrounding the Ti-O octahedron. (b) and (c) The asymmetric electric field in LAO induces an increase of the electrostatic potential energy away from the interface, and further causes band bending of LAO in both (110) and (001) interfaces. The LAO overlayer is 6 ML. (d) and (e) For more thick LAO overlayer in (110) and (001) interfaces, La vacancies can make the increased potential energy converge to a stable state. The valences of La, Al, O, and Sr are not marked out.

STO core level cannot be detected and the band bending should be determined by the end of the upward tail after the saturation.

APPENDIX B: VALENCE BAND OFFSET

We choose the Ti $2p_{3/2}$ in STO substrate and the Al $2p$ in LAO overlayer to determine the VBO of samples with different LAO overlayer thickness. The VBO (ΔE_V) can be obtained from the following equation:

$$\Delta E_V^{\mathrm{Al-Ti}} = (E_{\mathrm{Al}\,2p} - E_V)_{\mathrm{LAO}} - (E_{\mathrm{Ti}\,2p3/2} - E_V)_{\mathrm{STO}} + (E_{\mathrm{Ti}\,2p3/2} - E_{\mathrm{Al}\,2p})_{\mathrm{HJ}}, \quad \text{(B1)}$$

where $(E_{\mathrm{Al}\,2p} - E_V)_{\mathrm{LAO}}$ and $(E_{\mathrm{Ti}\,2p3/2} - E_V)_{\mathrm{STO}}$ are the LAO and STO bulk constants, which represent the energy differences between core level (Ti $2p_{3/2}$, Al $2p$) and valence band maximum (VBM, E_V) in LAO or STO. $(E_{\mathrm{Ti}\,2p3/2} - E_{\mathrm{Al}\,2p})_{\mathrm{HJ}}$ is core level energy difference measured from (110) LAO/STO heterojunction (Fig. 8). All the above values are the energy difference, so they were not affected by the residual charge effect.

The calculated VBO [see Fig. 3(c) in the main text] changes from negative to positive as LAO thickens. Based on this, the discrepancies of reported VBO of (001) LAO/STO in the literatures (e.g., 0.25 eV by Yoshimatsu *et al.* [49], zero or positive by Chambers *et al.* [41], negative by Drera *et al.* [62]) can be well explained.

Negative VBO signifies the VBM of LAO is more deeply bound than that of STO and the positive VBO is opposite. So the change of VBO from negative to positive indicates

that the VBM of LAO goes up in reference to that of STO away from the interface with increasing LAO thickness. The VBM value of STO, 3.00 ± 0.1 eV, was determined by using 0.7 wt.% Nb doped (110) STO substrates with a standard linear extrapolation of the leading edges of valence spectra to the base line [63,64]. It was well consistent with the value reported in Ref. [49] and the Nb-doped STO had also been used to determine the VBM of STO in Ref. [41]. The VBM of LAO can be determined to be about 2.73 eV from the data shown in Fig. 3(d) in the main text which is similar to the reported value [2.6 ± 0.1 eV for (001) LAO] in Ref. [65].

APPENDIX C: METHOD TO ESTIMATE THE WIDTH OF THE BAND BENDING

Normally, the shift of the core level with increasing thickness of the LAO overlayer is used to determine the value of the band bending. We can also estimate the width of the band bending based on the upward-tail phenomenon of Ti $2p_{3/2}$ described in Appendix A. As shown in Fig. 3(b) of the main text and the Fig. 7(a), the Ti $2p_{3/2}$ shifts to higher binding energy as the LAO becomes thicker, nearly saturates at about 6−10 ML, then turns upward again up to 18 ML. This upward shift after the saturation means that the investigation depth of XPS just covers the whole region of the bending when the LAO is 10 ML; with increase of the LAO overlayer, the investigation depth of XPS covers less and less of the region of band bending; the XPS signal becomes quite weak after 18 ML and finally vanishes at 25 ML (data not shown). So the thickness of the subsequent LAO overlayers from 10 ML to 18−25 ML is about equal to the width of the region of band bending, i.e., 2−4 nm. According to the literature [4,33,58,59], this value is reasonable at room temperature for our (110) LAO/STO samples grown in 10^{-4} mbar of oxygen with post-deposition annealing.

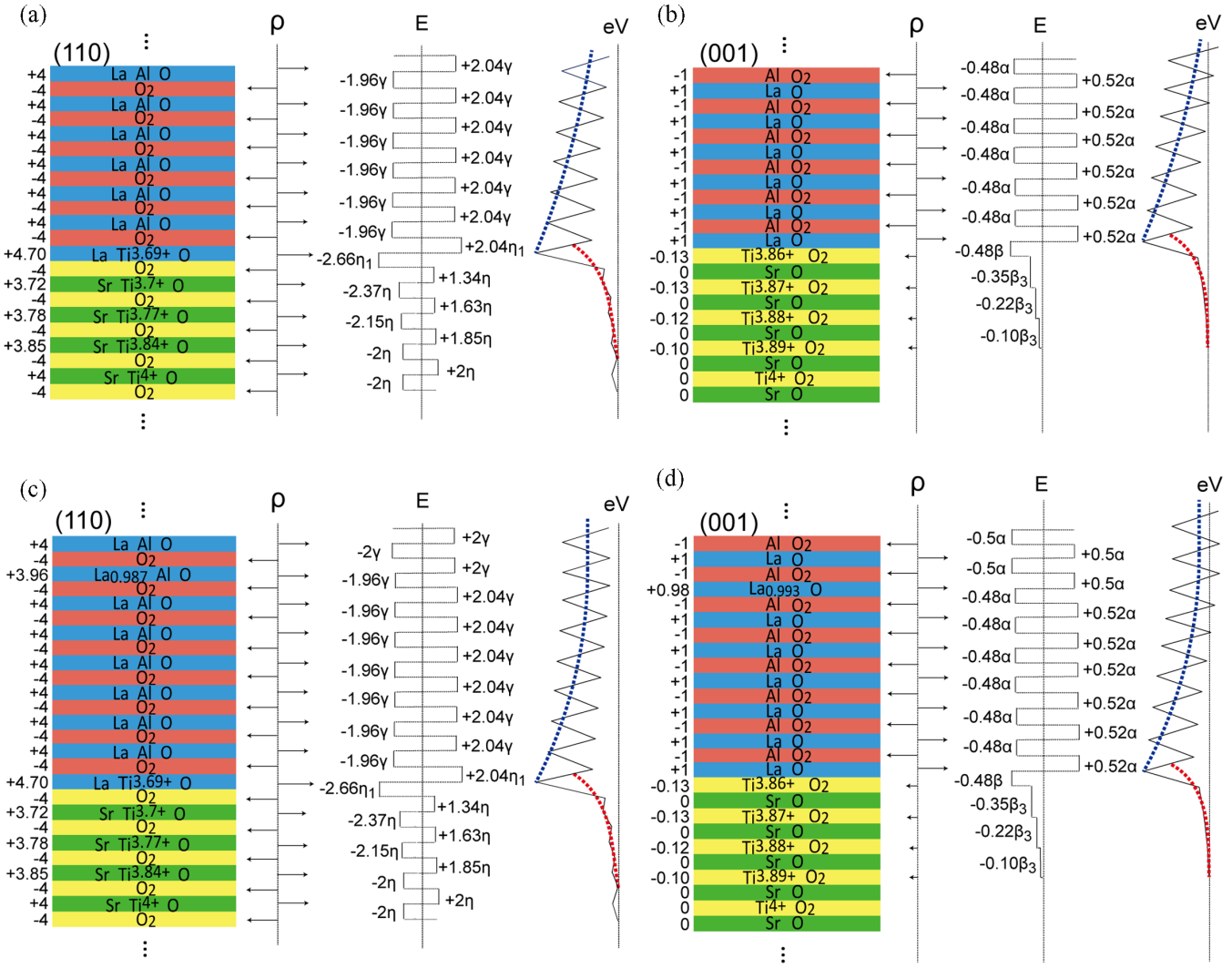

FIG. 10. (Color online) Explanation of band bending of LAO for the intrinsic coexistence of La and Ti. (a) and (b) after amending, only 96% electrons to change the valence of Ti, so the electric field of LAO was not totally eliminated, then induces band bending of LAO. (c) and (d) La vacancies can be introduced to make the increased potential energy converge to a stable state. The valences of La, Al, O, and Sr are not marked out.

APPENDIX D: EXPLANATION OF BAND BENDING OF LAO

In the main text, we have supposed that all the electrons supplied by La occupation of Sr were transferred to Ti to reduce its valence; this is an ideal model. It is closer to reality that only a part of the electrons play such a role. In the following, we suppose that the proportion of such a part is 96% of the total electrons supplied by La substitution of Sr. According to this amendment, the valence of Ti would decrease from +4 to +3.04 in proportion to the ratio of La/Sr surrounding the Ti-O octahedron as shown in Fig. 9(a). Therefore, the coexistence of La and Ti in ABO_3 perovskite unit cells at the interface can also generate a local asymmetric electric field in LAO for both (110) and (001) heterojunctions, as illustrated in Fig. 9(b) and Fig. 9(c), resulting in band bending at LAO sides. The calculated value of band bending is about 0.46 eV for (110) at 6 ML LAO overlayer [Fig. 9(b)], which is well consistent with our experimental result [$\sim$0.50 eV at 6 ML LAO, see Fig. 3(b) in the main text, the core level shift of Al $2p$]. For more LAO overlayers, just introduce La deficiencies in LAO layers, as shown in Fig. 9(d) and Fig. 9(e); the increased potential energy would converge to a stable state, avoiding the polar catastrophe. La deficiency in LAO side has also been reported to contribute to the formation of the 2DEG [26,66], so it is reasonable that we introduce La vacancies in our model.

For the situation of the intrinsic coexistence of La and Ti at both (001) and (110) LAO/STO interfaces, the band bending of the LAO sides can also be well explained using the above amendment. The results are shown in Fig. 10.

APPENDIX E: CALCULATION OF THE VALUE OF STATIC FIELD AND POTENTIAL ENERGY

We calculated the values of static field and potential energy by assuming an infinite plane-parallel capacitor structure of atomic layers. The value of static field is obtained using $E = \frac{ne}{\varepsilon_r \varepsilon_0 s}$, for (110) LAO/STO interfaces $s = \sqrt{2}a^2$, for (001) LAO/STO interfaces $s = a^2$, a is the lattice constant, n is the integral sheet charge for very infinite plane-parallel capacitor structure constructed by two atomic layers, e is the electron charge, and ε_r and ε_0 are the relative dielectric constant of the material and vacuum dielectric constant. The ε_r at room temperature is 300, 20, and 24 for STO [67], LTO [68], and LAO [69], respectively. For the intermixing layer, $La_{1-x}Sr_xTiO_3$, we assume that its ε_r depends on the concentration of La. We fit the dependencies based on three data: 300 for STO, 20 for LTO, and 90 for $La_{2/3}TiO_3$ [70]. The value of the static field is labeled as $n\alpha$, $n\beta$, $n\gamma$, or $n\eta$, in Figs. 6, 9, and 10. Each value of n for every atomic layer has been given out in the labeled value of the local asymmetric electric field of Figs. 6, 9, and 10. α, β, γ, η are constants deduced by $\frac{e}{\varepsilon_r \varepsilon_0 s}$, i.e., $\gamma = 3.49\times10^9$ V/m, $\eta_1 = 4.19\times10^9$ V/m, $\eta_2 = 1.19\times10^9$ V/m, $\eta_3 = 3.99\times10^8$ V/m, $\eta = 2.79\times10^8$ V/m, $\alpha = 4.94\times10^9$ V/m, $\beta = 5.93\times10^9$ V/m, $\beta_1 = 1.69\times10^9$ V/m, $\beta_2 = 5.64\times10^8$ V/m, $\beta_3 = 3.95\times10^8$ V/m.

The potential energy (the value of band bending) can be obtained by computing the integral for E.

[1] H. Y. Hwang, Y. Iwasa, M. Kawasaki, B. Keimer, N. Nagaosa, and Y. Tokura, Nat. Mater. **11**, 103 (2012).

[2] M. Bibes, J. E. Villegas, and A. Barthélémy, Adv. Phys. **60**, 5 (2011).

[3] A. Ohtomo and H. Y. Hwang, Nature (London) **427**, 423 (2004).

[4] N. Nakagawa, H. Y. Hwang, and D. A. Muller, Nat. Mater. **5**, 204 (2006).

[5] S. Thiel, G. Hammerl, A. Schmehl, C. W. Schneider, and J. Mannhart, Science **313**, 1942 (2006).

[6] M. Huijben, G. Rijnders, D. H. A. Blank, S. Bals, S. V. Aert, J. Verbeeck, G. V. Tendeloo, A. Brinkman, and H. Hilgenkamp, Nat. Mater. **5**, 556 (2006).

[7] A. D. Caviglia, S. Gariglio, N. Reyren, D. Jaccard, T. Schneider, M. Gabay, S. Thiel, G. Hammerl, J. Mannhart, and J.-M. Triscone, Nature (London) **456**, 624 (2008).

[8] C. Cen, S. Thiel, G. Hammerl, C. W. Schneider, K. E. Andersen, C. S. Hellberg, J. Mannhart, and J. Levy, Nat. Mater. **7**, 298 (2008).

[9] M. Basletic, J.-L. Maurice, C. Carretero, G. Herranz, O. Copie, M. Bibes, E. Jacquet, K. Bouzehouane, S. Fusil, and A. Barthelemy, Nat. Mater. **7**, 621 (2008).

[10] J. Mannhart and D. G. Schlom, Science **327**, 1607 (2010).

[11] N. Reyren, S. Thiel, A. D. Caviglia, L. F. Kourkoutis, G. Hammerl, C. Richter, C. W. Schneider, T. Kopp, A.-S. Rüetschi, D. Jaccard, M. Gabay, D. A. Muller, J.-M. Triscone, and J. Mannhart, Science **317**, 1196 (2007).

[12] J. Biscaras, N. Bergeal, S. Hurand, C. Feuillet-Palma, A. Rastogi, R. C. Budhani, M. Grilli, S. Caprara, and J. Lesueur, Nat. Mater. **12**, 542 (2013).

[13] C. Richter, H. Boschker, W. Dietsche, E. Fillis-Tsirakis, R. Jany, F. Loder, L. F. Kourkoutis, D. A. Muller, J. R. Kirtley, C. W. Schneider, and J. Mannhart, Nature (London) **502**, 528 (2013).

[14] A. Brinkman, M. Huijben, M. van Zalk, J. Huijben, U. Zeitler, J. C. Maan, W. G. van der Wiel, G. Rijnders, D. H. A. Blank, and H. Hilgenkamp, Nat. Mater. **6**, 493 (2007).

[15] A. J. Millis, Nat. Phys. **7**, 749 (2011).

[16] B. Kalisky, J. A. Bert, B. B. Klopfer, C. Bell, H. K. Sato, M. Hosoda, Y. Hikita, H. Y. Hwang, and K. A. Moler, Nat. Commun. **3**, 922 (2012).

[17] S. Banerjee, O. Erten, and M. Randeria, Nat. Phys. **9**, 626 (2013).

[18] M. Gabay and J.-M. Triscone, Nat. Phys. **9**, 610 (2013).

[19] D. A. Dikin, M. Mehta, C. W. Bark, C. M. Folkman, C. B. Eom, and V. Chandrasekhar, Phys. Rev. Lett. **107**, 056802 (2011).

[20] L. Li, C. Richter, J. Mannhart, and R. C. Ashoori, Nat. Phys. **7**, 762 (2011).

[21] J. A. Bert, B. Kalisky, C. Bell, M. Kim, Y. Hikita, H. Y. Hwang, and K. A. Moler, Nat. Phys. **7**, 767 (2011).

[22] M. L. Reinle-Schmitt, C. Cancellieri, D. Li, D. Fontaine, M. Medarde, E. Pomjakushina, C. W. Schneider, S. Gariglio, P. Ghosez, J.-M. Triscone, and P. R. Willmott, Nat. Commun. **3**, 932 (2012).

[23] J. N. Eckstein, Nat. Mater. **6**, 473 (2007).

[24] P. R. Willmott, S. A. Pauli, R. Herger, C. M. Schlepütz, D. Martoccia, B. D. Patterson, B. Delley, R. Clarke, D. Kumah, C. Cionca, and Y. Yacoby, Phys. Rev. Lett. **99**, 155502 (2007).

[25] G. Singh-Bhalla, C. Bell, J. Ravichandran, W. Siemons, Y. Hikita, S. Salahuddin, A. F. Hebard, H. Y. Hwang, and R. Ramesh, Nat. Phys. **7**, 80 (2011).

[26] E. Breckenfeld, N. Bronn, J. Karthik, A. R. Damodaran, S. Lee, N. Mason, and L. W. Martin, Phys. Rev. Lett. **110**, 196804 (2013).

[27] Z. Q. Liu, C. J. Li, W. M. Lü, X. H. Huang, Z. Huang, S. W. Zeng, X. P. Qiu, L. S. Huang, A. Annadi, J. S. Chen, J. M. D. Coey, T. Venkatesan, and Ariando, Phys. Rev. X **3**, 021010 (2013).

[28] J. Lee and A. A. Demkov, Phys. Rev. B **78**, 193104 (2008).

[29] Y. Segal, J. H. Ngai, J. W. Reiner, F. J. Walker, and C. H. Ahn, Phys. Rev. B **80**, 241107 (2009).

[30] R. Pentcheva and W. E. Pickett, J. Phys.: Condens. Matter **22**, 043001 (2010).

[31] M. Takizawa, S. Tsuda, T. Susaki, H. Y. Hwang, and A. Fujimori, Phys. Rev. B **84**, 245124 (2011).

[32] G. Berner, A. Müller, F. Pfaff, J. Walde, C. Richter, J. Mannhart, S. Thiess, A. Gloskovskii, W. Drube, M. Sing, and R. Claessen, Phys. Rev. B **88**, 115111 (2013).

[33] M. Sing, G. Berner, K. Goß, A. Müller, A. Ruff, A. Wetscherek, S. Thiel, J. Mannhart, S. A. Pauli, C. W. Schneider, P. R. Willmott, M. Gorgoi, F. Schäfers, and R. Claessen, Phys. Rev. Lett. **102**, 176805 (2009).

[34] A. Savoia, D. Paparo, P. Perna, Z. Ristic, M. Salluzzo, F. Miletto Granozio, U. Scotti di Uccio, C. Richter, S. Thiel, J. Mannhart, and L. Marrucci, Phys. Rev. B **80**, 075110 (2009).

[35] Y. Mukunoki, N. Nakagawa, T. Susaki, and H. Y. Hwang, Appl. Phys. Lett. **86**, 171908 (2005).

[36] G. Herranz, F. Sánchez, N. Dix, M. Scigaj, and J. Fontcuberta, Sci. Rep. **2**, 758 (2012).

[37] A. Annadi, Q. Zhang, X. Renshaw Wang, N. Tuzla, K. Gopinadhan, W. M. Lü, A. Roy Barman, Z. Q. Liu, A. Srivastava, S. Saha, Y. L. Zhao, S. W. Zeng, S. Dhar, E. Olsson, B. Gu, S. Yunoki, S. Maekawa, H. Hilgenkamp, T. Venkatesan, and Ariando, Nat. Commun. **4**, 1838 (2013).

[38] Y.-L. Han, S.-C. Shen, J. You, H.-O. Li, Z.-Z. Luo, C.-J. Li, G.-L. Qu, C.-M. Xiong, R.-F. Dou, L. He, D. Naugle, G.-P. Guo, and J.-C. Nie, Appl. Phys. Lett. **105**, 192603 (2014).

[39] G. Herranz, G. Singh, N. Bergeal, A. Jouan, J. Lesueur, J. Gázquez, M. Varela, M. Scigaj, N. Dix, F. Sánchez, and J. Fontcuberta, Nat. Commun. **6**, 6028 (2015).

[40] A. S. Kalabukhov, Y. A. Boikov, I. T. Serenkov, V. I. Sakharov, V. N. Popok, R. Gunnarsson, J. Börjesson, N. Ljustina, E. Olsson, D. Winkler, and T. Claeson, Phys. Rev. Lett. **103**, 146101 (2009).

[41] S. A. Chambers, M. H. Engelhard, V. Shutthanandan, Z. Zhu, T. C. Droubay, L. Qiao, P. V. Sushko, T. Feng, H. D. Lee, T. Gustafsson, E. Garfunkel, A. B. Shah, J.-M. Zuo, and Q. M. Ramasse, Surf. Sci. Rep. **65**, 317 (2010).

[42] L. Qiao, T. C. Droubay, T. Varga, M. E. Bowden, V. Shutthanandan, Z. Zhu, T. C. Kaspar, and S. A. Chambers, Phys. Rev. B **83**, 085408 (2011).

[43] R. Yamamoto, C. Bell, Y. Hikita, H. Y. Hwang, H. Nakamura, T. Kimura, and Y. Wakabayashi, Phys. Rev. Lett. **107**, 036104 (2011).

[44] Y. Fujishima, Y. Tokura, T. Arima, and S. Uchida, Phys. Rev. B **46**, 11167 (1992).

[45] M. Takizawa, H. Wadati, K. Tanaka, M. Hashimoto, T. Yoshida, A. Fujimori, A. Chikamatsu, H. Kumigashira, M. Oshima, K. Shibuya, T. Mihara, T. Ohnishi, M. Lippmaa, M. Kawasaki, H. Koinuma, S. Okamoto, and A. J. Millis, Phys. Rev. Lett. **97**, 057601 (2006).

[46] W. Siemons, G. Koster, H. Yamamoto, W. A. Harrison, G. Lucovsky, T. H. Geballe, D. H. A. Blank, and M. R. Beasley, Phys. Rev. Lett. **98**, 196802 (2007).

[47] G. Herranz, M. Basletić, M. Bibes, C. Carrétéro, E. Tafra, E. Jacquet, K. Bouzehouane, C. Deranlot, A. Hamzić, J.-M. Broto, A. Barthélémy, and A. Fert, Phys. Rev. Lett. **98**, 216803 (2007).

[48] R. Bachelet, F. Valle, I. C. Infante, F. Sanchez, and J. Fontcuberta, Appl. Phys. Lett. **91**, 251904 (2007).

[49] K. Yoshimatsu, R. Yasuhara, H. Kumigashira, and M. Oshima, Phys. Rev. Lett. **101**, 026802 (2008).

[50] E. Slooten, Z. Zhong, H. J. A. Molegraaf, P. D. Eerkes, S. de Jong, F. Massee, E. van Heumen, M. K. Kruize, S. Wenderich, J. E. Kleibeuker, M. Gorgoi, H. Hilgenkamp, A. Brinkman, M. Huijben, G. Rijnders, D. H. A. Blank, G. Koster, P. J. Kelly, and M. S. Golden, Phys. Rev. B **87**, 085128 (2013).

[51] G. Kresse and J. Furthmüller, Phys. Rev. B **54**, 11169 (1996).

[52] A. Hashibon, C. Elsässer, Y. Mishin, and P. Gumbsch, Phys. Rev. B **76**, 245434 (2007).

[53] J.-M. Albina, M. Mrovec, B. Meyer, and C. Elsässer, Phys. Rev. B **76**, 165103 (2007).

[54] A. Ohtomo, D. A. Muller, J. L. Grazul, and H. Y. Hwang, Nature (London) **419**, 378 (2002).

[55] S. Okamoto, A. J. Millis, and N. A. Spaldin, Phys. Rev. Lett. **97**, 056802 (2006).

[56] H. W. Jang, D. A. Felker, C. W. Bark, Y. Wang, M. K. Niranjan, C. T. Nelson, Y. Zhang, D. Su, C. M. Folkman, S. H. Baek, S. Lee, K. Janicka, Y. Zhu, X. Q. Pan, D. D. Fong, E. Y. Tsymbal, M. S. Rzchowski, and C. B. Eom, Science **331**, 886 (2011).

[57] This definition is reasonable because the (110) surface of STO substrate is in favor of lacking Sr, which is supported by DFT calculations (e.g., Ref. [37]) and some experiment [e.g., A. Biswas *et al.*, Appl. Phys. Lett. **98**, 051904 (2011); Z. Wang *et al.*, Phys. Rev. Lett. **111**, 056101 (2013)], so when LAO is grown on the (110) STO substrate, an intrinsic coexistence of La and Ti would be formed at the interface without extra atomic diffusion. In addition, our calculation of mechanical interface stability is energetically in favor of (110) LAO/LTO-STO supercell to (110) LAO/STO supercell.

[58] M. Stengel, Phys. Rev. Lett. **106**, 136803 (2011).

[59] O. Copie, V. Garcia, C. Bödefeld, C. Carrétéro, M. Bibes, G. Herranz, E. Jacquet, J.-L. Maurice, B. Vinter, S. Fusil, K. Bouzehouane, H. Jaffrès, and A. Barthélémy, Phys. Rev. Lett. **102**, 216804 (2009).

[60] W. Tang, E. Sanville, and G. Henkelman, J. Phys.: Condens. Matter **21**, 084204 (2009).

[61] M. S. Park, S. H. Rhim, and A. J. Freeman, Phys. Rev. B **74**, 205416 (2006).

[62] G. Drera, G. Salvinelli, A. Brinkman, M. Huijben, G. Koster, H. Hilgenkamp, G. Rijnders, D. Visentin, and L. Sangaletti, Phys. Rev. B **87**, 075435 (2013).

63 S. A. Chambers, Y. Liang, Z. Yu, R. Droopad, J. Ramdani, and K. Eisenbeiser, Appl. Phys. Lett. **77**, 1662 (2000).

[64] J. R. Waldrop, R. W. Grant, S. P. Kowalczyk, and E. A. Kraut, J. Vac. Sci. Technol. Vac. Surf. Films **3**, 835 (1985).

[65] J. Y. Yang, Y. Sun, P. Lv, L. He, R. F. Dou, C. M. Xiong, and J. C. Nie, Appl. Phys. A **105**, 1017 (2011).

[66] M. P. Warusawithana, C. Richter, J. A. Mundy, P. Roy, J. Ludwig, S. Paetel, T. Heeg, A. A. Pawlicki, L. F. Kourkoutis, M. Zheng, M. Lee, B. Mulcahy, W. Zander, Y. Zhu, J. Schubert, J. N. Eckstein, D. A. Muller, C. S. Hellberg, J. Mannhart, and D. G. Schlom, Nat. Commun. **4**, 2351 (2013).

[67] H.-M. Christen, J. Mannhart, E. J. Williams, and C. Gerber, Phys. Rev. B **49**, 12095 (1994).

[68] T. Hato, A. Yoshida, C. Yoshida, H. Suzuki, and N. Yokoyama, Appl. Phys. Lett. **70**, 2900 (1997).

[69] S.-Y. Cho, I.-T. Kim, and K. S. Hong, J. Mater. Res. **14**, 114 (1999).

[70] F. Azough, W. Wang, and R. Freer, J. Am. Ceram. Soc. **92**, 2093 (2009).